Composites Part B 140 (2018) 83–90

Contents lists available at ScienceDirect

Composites Part B

journal homepage: www.elsevier.com/locate/compositesb

Dielectric properties and thermal conductivity of epoxy composites using core/shell structured Si/SiO_2/Polydopamine

Zhengdong Wang[a], Yonghong Cheng[a,*], Mengmeng Yang[a], Jialiang Huang[a], Daxian Cao[a], Siyu Chen[a], Qian Xie[a], Wanxi Lou[a], Hongjing Wu[b]

[a] Center of Nanomaterials for Renewable Energy, State Key Laboratory of Electrical Insulation and Power Equipment, Xi'an Jiaotong University, Xi'an 710049, China
[b] Department of Applied Physics, Northwestern Polytechnical University, Xi'an 710072, China

ARTICLE INFO

Keywords:
Core-shell
Si/SiO_2/Polydopamine
Epoxy composites
Dielectric properties
Thermal conductivity

ABSTRACT

We report the fabrication of epoxy-based composites using well-designed core/shell Si/SiO_2 (denoted as Si*) and core/shell/shell structured Si/SiO_2/Polydopamine (denoted as Si*@PDA) particles as fillers, which exhibit improved dielectric properties and thermal conductivity. Using the core-shell Si* and Si*@PDA particles as fillers in the epoxy-based composites, the dielectric loss tangent is remarkably suppressed and the volume resistivity is apparently enhanced, as compared with that using raw Si particles as fillers. Moreover, the Si*@PDA composites have higher dielectric constant and lower loss tangent. For instance, the dielectric constant of Si*@PDA/epoxy composite with 33.8 vol% filler content is up to 19.8 at room temperature at 100 Hz, which is nearly 5.3 times of that of the pure epoxy polymer (3.4), while its loss tangent is only 0.085. Additionally, the core-shell particle-based composites still possess a high thermal conductivity.

1. Introduction

Materials with high dielectric constant but low dielectric loss have attracted considerable attentions owing to the rapid development of electronic and electrical industry, such as energy storage devices, embedded capacitors, electric accessories and artificial muscles and skins [1–3]. Recently, polymer-matrix-based composites with high dielectric constant and low dielectric loss have been widely studied and applied as structural materials because of their excellent properties, such as good flexibility, easy processability, lightweight, and ultralow dielectric loss in comparison with the traditional inorganic high-k materials [4,5]. Epoxy resin, which possesses many excellent characteristics including superior electrical insulating, high thermal and chemical stabilities, has been well-recognized as a good candidate for structural capacitors and embedded components [4,6,7]. However, the low dielectric constant of epoxy limits its practical application. To increase the dielectric constant of epoxy resin, one important strategy is to design and fabricate organic-inorganic composites by incorporating high-k inorganic ceramic particles (ex., $BaTiO_3$, $CaCu_3Ti_4O_{12}$, $PbZrTiO_3$, $BaSrTiO_3$, etc.) into polymer matrix [8–10]. However, the enhancement of dielectric constant usually needs high loading of high-k particles, which may lose the flexibility of the polymer matrix. Nevertheless, the dilemma for using inorganic ceramic particles is that the increase of dielectric constant can be usually attained at the expense of the significant decrease in the flexibility of the polymer matrix, owing to high loading of high-k particles for high-k composites. Another approach for enhancing dielectric constant is to incorporate electrically conductive particles (Ag, Cu, Al, Zn and carbon fillers) into a polymer, leading to a significant high dielectric constant when the concentration of conductive fillers approaches the percolation threshold [1,2,4,11–16]. However, some applications of these composites in the field of electrical industry would be hindered owing to the accompanied high dielectric loss and electric conductivity.

Recently, core-shell particles as fillers have attracted increasing interest due to their desirable characteristics, such as high surface area, low density and good stability after shell protection, which have shown promising applications in drug delivery [17], catalysis [18], microwave absorption [19–22] and energy storage [1,2,23,24]. As compared with the conventional mixing methods, core-shell nanostructuring strategies are versatile and powerful tools for the design and synthesis of advanced high-k polymer nanocomposites [24]. In order to obtain high-k and low loss composites, various types of core-shell structures have been delicately designed via controlling and optimizing the microstructures and electrical properties of the particles. Coating insulating shells on conductive cores or polymer shells on ceramic cores have been widely used to prepare high-k polymer composites with low loss, such as CNTs@SiO_2 [25], Al@Al_2O_3 [1,16], $BaTiO_3$@HBP [26], $BaTiO_3$@PS [27] and so on.

* Corresponding author.
E-mail address: cyh@mail.xjtu.edu.cn (Y. Cheng).

https://doi.org/10.1016/j.compositesb.2017.12.004
Received 25 May 2017; Received in revised form 10 December 2017; Accepted 15 December 2017
Available online 16 December 2017

As compared with the conductive or the ceramic particles, Si particles are expected to be an excellent candidate for structural capacitors. First, Si is a very important semiconductor material, which shows a variety of applications in microelectronic devices, solar cells, and light-guided fiber materials [7,28]. The resistivity of Si is $2.52 \times 10^{-4}\,\Omega\,m$, which is relatively lower than that of the Silicon Carbide (SiC) or Silicon Nitride (Si_3N_4) counterparts. Besides, Si possesses high thermal conductivity (148 W/m K), low density (2.33 g/cm^3) and low cost. Apparently, Si is a better choice in increasing the dielectric constant and thermal conductivity of polymer matrix while keeping a relatively low density. In this work, we successfully decreased the dielectric loss while maintaining a high-k of the Si/polymer by coating Si particles with insulating layers of SiO_2 and PDA. A novel core-shell structured Si* particles were obtained by a facile thermal oxidation of Si under oxygen atmosphere, and the oxidized SiO_2 surface layer on individual Si particles was highly insulating and effectively blocked charge transport, which thus lowered the dielectric loss in the composites. Furthermore, surface coating of Si* particles with PDA layers were also conducted via the facile self-polymerization of dopamine, and interestingly the PDA effectively improved the interface adhesion between the filler and epoxy matrix, which led to greatly increased thermal conductivity, higher dielectric constant and lower dielectric loss at the same time. More importantly, the current study brought new insight into the design of advanced composites with simultaneous improvement of the overall dielectric properties and thermal conductivity, via the delicate core-shell engineering.

2. Experimental section

2.1. Materials

Micro-sized Si particles with irregular shape and an average size of 1 μm were bought from Guangzhou Yanrui Chemical industry Co. Ltd. The bisphenol A epoxy resin (E−828) along with anhydride hardener (MTHPA) and benzyldimethylamine (BDMA, serving as the accelerant) were purchased from Aladdin Reagent (shanghai) Co. Ltd., China. Dopamine hydrochloride (DPA-HCl, 98%) and tris (hydroxymethyl) aminomethane (Tris, 99%) were purchased from Sigma-Aldrich and used without further purification. Hydrochloric acid (HCl, 37 wt%) was provided by Shanghai Reagents Co. Ltd.

2.2. Preparation of Si/SiO_2 (Si*) and Si/SiO_2/Polydopamine (Si*@PDA) fillers

Core/shell Si/SiO_2 particles were prepared by thermal oxidation of the raw Si particles at 900 °C for 2 h in a tube furnace under an oxygen flow of 100 cm^3/min. In a typical synthesis of core/shell/shell Si/SiO_2/Polydopamine, 5.0 g Si/SiO_2 particles were dispersed in 200 mL Tris-HCl aqueous buffer solution (pH = 8.5) under ultrasound irradiation for 20 min, and then 0.2 g Dopamine-HCl was added and ultrasonically dispersed for another 10 min afterwards, the mixture was stirred vigorously at 60 °C for 24 h, and then the particles were collected by centrifugation at 9000 rpm for 15 min. The as-obtained products were re-dispersed in ethanol, and the mixture was centrifuged at 9000 rpm for 15 min. After washing with ethanol for three times, gray Si*@PDA particles were obtained and dried under vacuum at 60 °C for 24 h.

2.3. Preparation of epoxy-based composites

Certain amount of fillers was proportionally mixed with MTHPA (86 wt% of epoxy resin) and epoxy by mechanical stirring, which was continuously dispersed by ultrasonic bath at 60 °C until forming a stable suspension. Then BDMA (2 wt% of epoxy resin) was added into the above MTHPA/epoxy mixture, which was then transferred into a Planetary Centrifugal Mixer (Thinky USA Inc.) for further dispersion under the rapid rotation and vigorous mixing. Afterwards, the mixture solution was slowly poured into the stainless steel models and was degassed in vacuum drying oven for 30 min at 60 °C. After pre-curing at 100 °C for 2 h and the post-curing at 150 °C for 10 h in an oven, the samples were finally obtained and taken out from models after cooling down to room temperature.

2.4. Structure and property characterization

The phase structures of the samples were examined by X-ray diffraction (XRD) using as a Bruker D2 PHASER diffractometer. Thermal gravimetric analysis (TGA) was performed at a heating rate of 10 °C/min under nitrogen atmosphere. Differential scanning calorimetry (DSC, 200 F3, NETZSCH, Germany) was performed to study glass transition temperature (T_g) of the composites in a temperature range of 25–200 °C at a heating rate of 10 °C/min under nitrogen atmosphere. Morphological structures of the fillers and the composites were characterized using field emission scanning electron microscopy (FESEM, FEI QUANTA F250). The microstructures of the Si* and Si*@PDA were observed by FEI Tecnai G2 F20 S-TWIN transmission electron microscope (TEM). The thermal diffusivity (δ) and specific heat (C_p) were measured using a laser flash apparatus (LFA 467 Nanoflash, NETZSCH, Germany). The bulk density (ρ) was calculated on the basis of the length, width and height of the products. The thermal conductivity (λ) value was calculated according to the equation $\lambda = \delta\rho C_p$, which is determined by the thermal diffusivity, specific heat and bulk density. For the measurements, the samples were first cut into quadrate shape with area of $10 \times 10\,mm^2$ and thickness of 0.3 mm, and then the quadrate samples were coated with a layer of graphite by spraying before test. The volume resistance (R_V) of the samples was tested using a high resistance meter (Agilent 6517B). For dielectric property measurements, gold electrodes were first sputtered on both sides of epoxy-based composites using an auto fine coater, and a mask with eyelet of 3 mm in diameter was used. The dielectric properties of the composites were measured using a broadband dielectric spectrometer (CONCEPT 80, Novocontrol Technology Company, Germany) with an Alpha-A high-performance frequency analyzer in the frequency range of 10^{-1}-10^6 Hz.

3. Results and discussion

3.1. XRD and TGA analyses

Fig. 1a schematically illustrates the synthetic strategy of the Si* and Si*@PDA fillers and their epoxy composites. Fig. 2a compares the XRD patterns of pristine Si, Si* and Si*@PDA particles, and all the prominent peaks in the three sample can be indexed to the well-crystalline Si phase (JCPDS No.). Differently, a minor broad peak located at around 23° appears in the Si* and Si*@PDA samples, which can be attributed to amorphous SiO_2 layers formed after oxidation in air. According to the XRD analysis, no additional peaks in the PDA-coated Si* are observed because of the intrinsic amorphous structure of PDA. It's noteworthy to

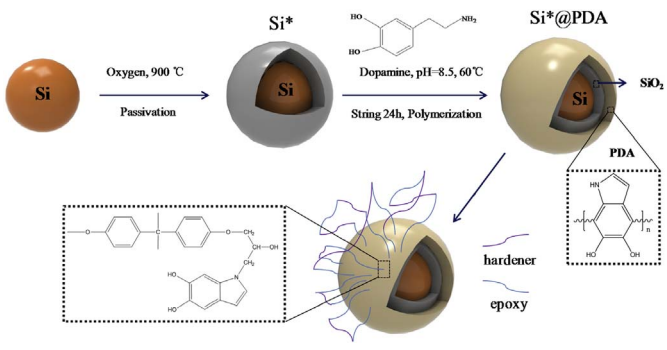

Fig. 1. Schematic illustration of the fabrication of Si* and Si*@PDA fillers and the epoxy composites.

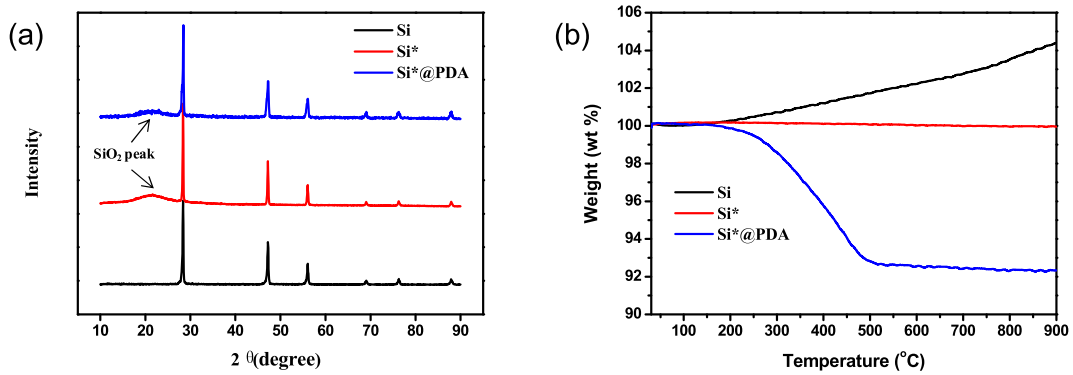

Fig. 2. (a) XRD patterns and (b) TGA curves of Si, Si* and Si*@PDA.

mention that both Si* and Si*@PDA exhibit intrinsic crystalline structure of silicon, indicating that the coating layers have no affection on the crystalline structure of Si. Moreover, the diffraction peak intensity of Si slightly decreases after the coating of amorphous SiO_2, while the XRD profile of the Si*@PDA ak becomes rough after the PDA functionalization as compared with Si*, which can be seen from the enlarged XRD patterns (Fig. S1). The amorphous PDA layer, which is coated on the surface of the Si* particles, results in the slightly weakened peak intensity.

Fig. 2b compares the TGA curves of Si, Si* and Si*@PDA samples. For the pristine Si, no weight loss is observed, indicating its purity with little absorbents. When increasing temperature at 200 °C above, steady weight increase is observed, which can be attributed to the oxidation of Si into SiO_2. As compared with pristine Si, the Si* sample shows no obvious weight change in the overall temperature range (25–900 °C), which is owing to the presence of a compact oxidation layer of SiO_2, thus further oxidation of Si particles is prevented. In contrast, owing to the coating of PDA layer on the Si* particles, the weight loss starts at 200 °C and becomes constant at 500 °C, indicating the complete decomposition of the polydopamine layers coated to the surface of the Si* particles [27]. Moreover, the content of polydopamine in the Si*@PDA composites is estimated to be approximately 7.5 wt%, which further confirms the successful wrapping of PDA on Si* particles.

3.2. SEM and TEM analyses

The morphologies of pristine Si and the core-shell structured Si* and Si*@PDA particles are shown in Fig. 3a–c, respectively. The bare Si particles show irregular shapes with diameters ranging from hundreds of nanometers to several micrometers. After calcination at 900 °C in air, the as-obtained Si* particles still maintain the morphology but showing well defined profiles, and it's observed that smaller particles are attached onto the surface of micro-particles. In contrast, the surface of the Si*@PDA particles becomes rough after coating with PDA, as compared with Si and Si* counterparts. Furthermore, TEM images of Si, Si* and Si*@PDA particles are compared, as shown in the insets of Fig. 3a–c. It's clearly observed that a conformal shell layer of SiO_2 (ca. 15 nm) is coated on the Si particle, and the SiO_2 shells show amorphous nature. After PDA functionalization, an additional rough layer of PDA with thickness of 5–10 nm is coated on the SiO_2 layer, forming the core-shell-shell of Si-SiO_2-PDA. TEM image (Fig. 3c) clearly confirms the successful non-covalent encapsulation of Si* particles by PDA via self-polymerization of dopamine [29]. The PDA layer shows a rough surface in comparison with that of inorganic particles, which may facilitate the strong adhesion with the epoxy matrix when using PDA-coated Si* particles as fillers.

The morphologies of the fracture surfaces of the Si/epoxy and Si*/epoxy composites with 18.0 vol% loading are compared in Fig. 3d and e. It's clearly observed that there are apparent voids and agglomerations in both Si/epoxy and Si*/epoxy composites, as shown in the magnified

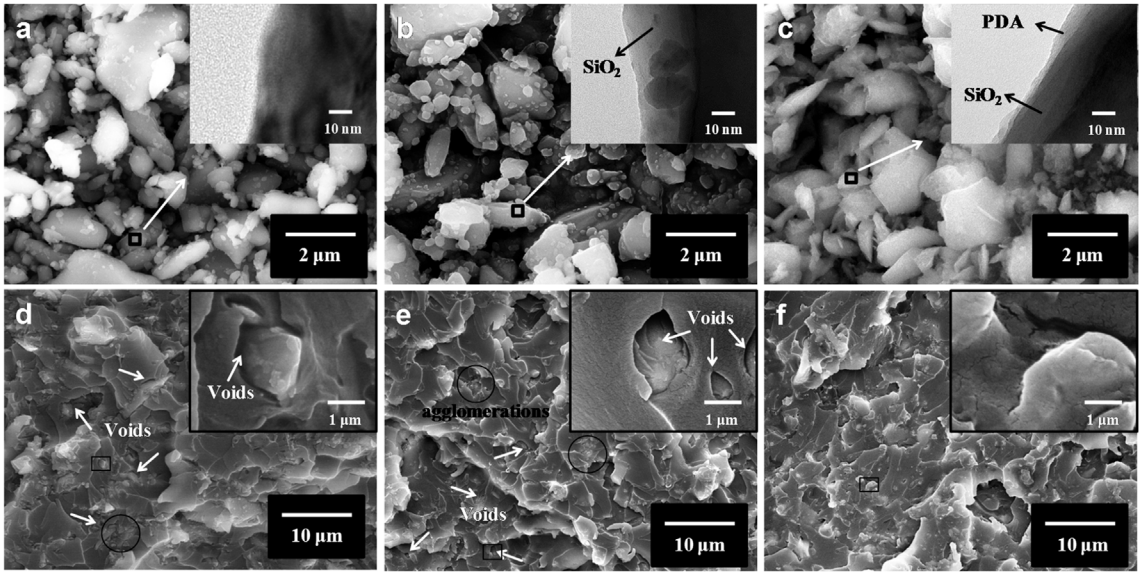

Fig. 3. SEM image of (a) Si, (b) Si* and (c) Si*@PDA samples with insets showing the corresponding TEM images. SEM images of the fracture surface of (d) 18.0 vol% Si/epoxy, (e) 18.0 vol% Si*/epoxy and (f) 18.0 vol% Si*@PDA/epoxy with insets showing the corresponding magnified images.

SEM images (insets of Fig. 3d and), which indicates the distinct incompatibility and poor interfacial bonding between Si (or Si*) particles and epoxy matrix. In contrast, Fig. 3f shows the interfacial contact between the Si*@PDA particles and the epoxy matrix. No obvious aggregation of the Si*@PDA particles in the composite can be observed in comparison with Si/epoxy and Si*/epoxy composites, and the boundary between Si*@PDA and epoxy looks hazy and indistinct in the composites, which shows a better contact with no apparent void structure (inset of Fig. 3f). Such composite facilitates the phonon transfer at the boundary area, which allows high thermal conductivity as compared with the Si*/epoxy composites. The good interfacial contact can be attributed to the special physicochemical characteristics of the coated PDA layer, which improves the interfacial adhesion when mixing with epoxy matrix. In addition, increasing the introducing amount of the three fillers (ex., 25.5 vol%) can significantly decrease the distance between fillers and epoxy matrix, in comparison with that of 18.0 vol% filler contents in the composites (Fig. S1). Generally, high filler loading is essential to achieve an appropriate level of thermal conductivity and effective dielectric permittivity in polymer-based composites. However, too high inorganic filler loading (35 vol%) would lead to the significant processing challenge, dramatically alter the mechanical behavior and increase the density of polymer-based composites. Hence, it's necessary to maintain a relatively low filler loading level in composites, in order to ensuring good flexibility.

3.3. Dielectric properties

Dielectric permittivity of a material is a factor which can reflect the charge storage ability of a capacitor and the material's dielectric properties when subjected to an external electric field. The effects of the content, surface treatment, and core-shell structure of Si particles as well as the frequency on the dielectric permittivity of the Si/epoxy composites are illustrated in Fig. 4. As expected, the dielectric permittivity increases with increasing the filler loading in epoxy in the frequency range of 10^{-1}-10^{6} Hz at room temperature for all the three systems. The Maxwell-Wanger-Sillars relaxation effect can be explained by the increment of dielectric permittivity related to the capture of free charges between the conductor and insulator or semiconductor and insulator in interfaces [13,14]. The dielectric permittivity of Si/epoxy composite increases steadily with increasing Si content in the range of 0–25.5 vol%. However, Si/epoxy composite varys greatly in magnitude at 33.8 vol% filler loading in comparison with the other two systems, similar to the dielectric behavior of percolative composites composed of insulating polymers and conductive fillers [30–34]. Dielectric permittivities of all the three composites show similar frequency dependence, and decrease slightly with increasing the frequency for the three systems. The reason can be attributed to the fact that interfacial polarization and orientation polarization of dipoles cannot keep synchronization under the external electric field, which account for the decrease of the dielectric constant [1,4]. It should be noted that the decline of the dielectric permittivity with varying frequency is more distinct for Si*@PDA/epoxy composite at low frequency because of the existence of coated PDA layer.

Sun et al. reported a kind of Si/epoxy nanocomposite by filling Si nanospheres into epoxy. In this composite, the dielectric permittivity was distinctly improved by introducing nano-Si and treated nano-Si [7]. In this work, we selected the micro-Si particles as the filler and achieved higher dielectric permittivity at same filler content. For nanocomposites, molecular motion, which contributes to the transfer of carriers and orientation of dipoles, is strongly restricted at the matrix/filler interface region [35,36]. This should be responsible for the lower dielectric permittivity in the nano-Si/epoxy composites. Fig. 4a shows that the dielectric permittivity of a composite with 5.4 vol% Si loading is 8.3, which is about 2.4 times of that of the pure epoxy at 100 Hz. When the loading of Si is lower than 33.8 vol%, the dielectric constant increases steadily. However, the dielectric constant rises from 20.9 (25.5 vol%) to 257.0 (33.8 vol%) at 100 Hz, indicating that the conductive network forms in the composites. In other words, the

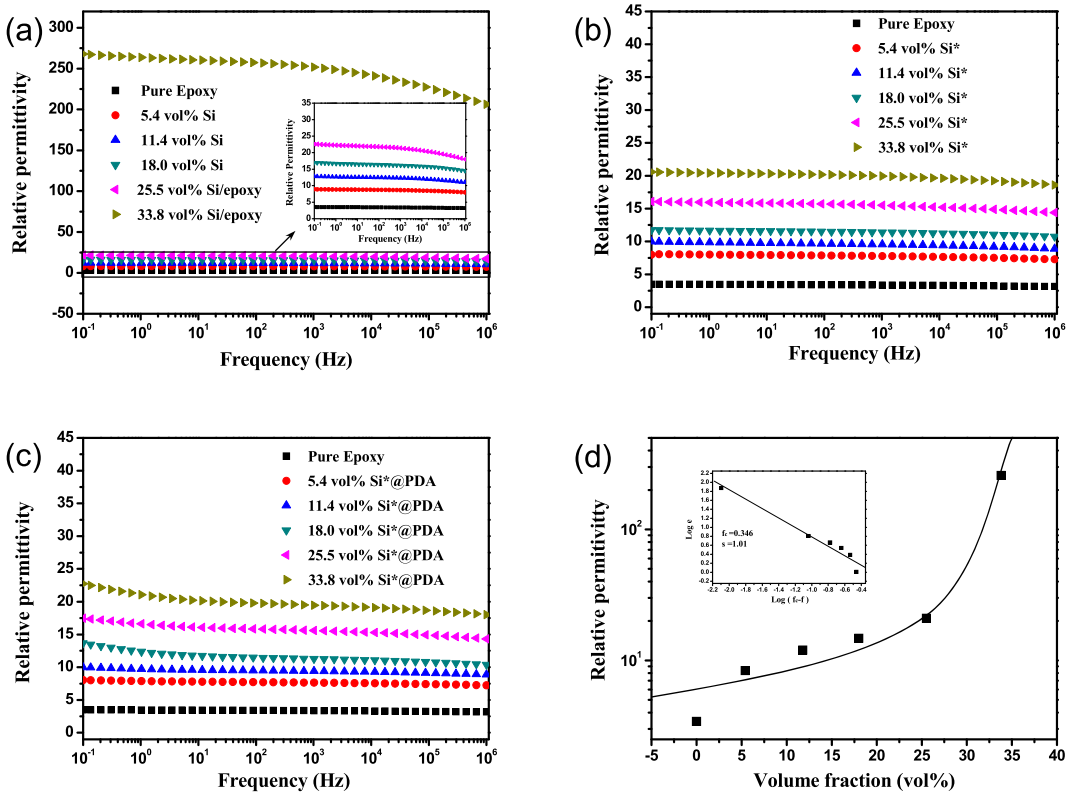

Fig. 4. Dielectric permittivity dependence on frequency and filler loading for the epoxy with 5.4–33.8 vol% (a) raw Si, (b) Si* and (c) Si*@PDA fillers. (d) Dielectric permittivity dependence on filler loading for the Si/epoxy composite with inset showing the best fits of the permittivity according to Eq. (1).

percolation threshold locates in the composite with filler loading between 25.5 vol% and 33.8 vol%. The high percolation threshold can be ascribed to the micro-scale and blocky structure against the formation of partial connectivity. A large quantity of blocked electric charges accumulate in the interfacial region between Si particles and epoxy matrix, resulting in a distinct increase in dielectric permittivity when increasing Si content. For insulating polymers filling with conductive or semi-conductive fillers, the variations of dielectric permittivity with filler content follow a percolation theory as the volume fraction of the conductive or semi-conductive fillers approaches to the percolation threshold, whilst the fillers form a good connectivity. As an excellent semiconductor material, Si exhibits similar percolation phenomenon with conduction similar with that of metals, carbon nanotubes and graphenes, etc.

The power law expresses the increase of the dielectric permittivity near the percolation threshold as below [13,37]:

$$\varepsilon_{eff} \propto (f_c - f_{si})^{-s} \quad \text{for} \quad f_c \geq f_{si} \tag{1}$$

where ε_{eff} is the effective dielectric permittivity and s is the corresponding critical exponent. The dielectric permittivity as a function of the volume fraction of Si shows explicit power characteristic as described by the power law. From the inset of Fig. 4d, we can get the values $f_c \approx 0.346$ and $s \approx 1.01$, according to Eq. (1). The critical exponent here, $s = 1.01$, is consistent with the universal one. It's noted that the dielectric loss also shows a large variation near the percolation threshold (Fig. 5d) [37].

Fig. 4b shows the dielectric permittivity of the Si*/epoxy composite as a function of filler loading and frequency at room temperature. The dielectric permittivity increases steadily with increasing Si* content, and shows a rather weak frequency dependence, indicating that there is deficient accumulation of charges at the interfaces. The increase of the dielectric permittivity can be attributed to the enhanced interfacial polarization. As compared with the Si/epoxy composite, no dramatic increase in the dielectric permittivity was detected for both Si*/epoxy and Si*@PDA/epoxy (Fig. 4c), even the filler loading was increased up to 33.8 vol%. This can be attributed to the formation of the oxidized SiO_2 shells on the surface of Si cores, and the SiO_2 insulating interface effectively prevents direct contact between adjacent Si cores and plays a decisive role in blocking the carrier transfer [7,28]. By the same token, the coated PDA layer in the Si*@PDA/epoxy composite also plays a similar role in blocking the free carrier migration. Moreover, the Si*@PDA/epoxy composite exhibits higher dielectric constant than that of the Si*/epoxy composite, owing to the multifold interfacial polarizations induced by oxidized SiO_2 and coated PDA layer, thus resulting in the stronger interfacial polarization. Therefore, in this work, for a given content of fillers, the dielectric permittivity values are in a trend of Si/epoxy > Si*@PDA/epoxy > Si*/epoxy.

Fig. 5 displays the dependence of dielectric loss on frequency at room temperature for the Si/epoxy, Si*/epoxy and Si*@PDA/epoxy composites. The dielectric loss for all the three samples decreases at the low frequency range from 10^{-1}–10^{2} Hz, and then increases remarkably over 10^{2} Hz. The low-frequency dielectric response would reflect the representative interface polarization behavior, rooting in the macroscopic interface of the different multiphase structures. In contrast, the high-frequency dielectric response can be ascribed to the C-F dipole orientation polarization of the composites according to Debye relaxation theory [13]. The dielectric properties of polymers when incorporated by conductors or semiconductors are largely dependent on the electrical properties of the fillers, which significantly affect the accumulation and migration of free carrier at the interfacial region between the filler and the polymer matrix. For the Si/epoxy composite, the dielectric loss increases with increasing the volume fractions of the Si content. There is no significant variation in the dielectric loss behaviors when Si loading is up to 25.5 vol%. However, the dielectric loss increases dramatically over the testing frequency range with increasing the filler content up to 33.8 vol%, principally resulting from the sharp conduction increase induced by the percolation effect. At a high Si loading, there are partial connections and networks of the fillers (Fig. S2), resulting in the rapid increase in dielectric loss. However, no drastic variation in the dielectric loss for the Si*/epoxy and Si*@PDA/

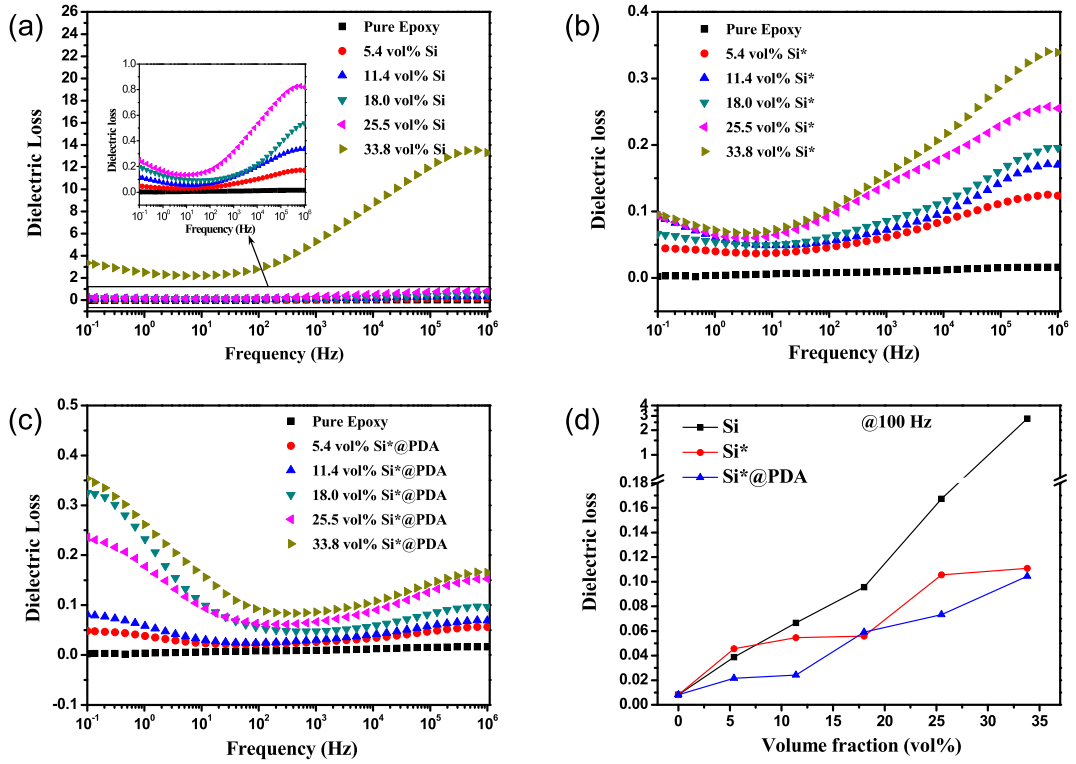

Fig. 5. Dielectric loss dependence on frequency and filler loading for the epoxy with 5.4–33.8 vol% (a) raw Si, (b) Si*, (c) Si*@PDA fillers; (d) Dielectric loss dependence on filler loading for the three composites.

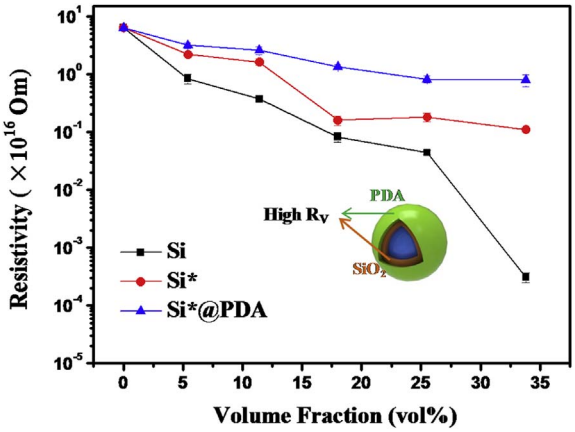

Fig. 6. Relationship between DC volume resistivity and filler loading for the three composites.

epoxy composites was observed at the content of 33.8 vol%, owing to the insulating layer of oxidized SiO_2 and coated PDA shell, resulting in a high volume resistivity, as revealed in Fig. 6.

As shown in Fig. 5b, Si*/epoxy composite shows a remarkably decreased dielectric loss as compared with the Si/epoxy composite, and the maximum dielectric loss value still remains a fairly low level. The dielectric loss of the Si*/epoxy composite with 33.8 vol% filler fraction is only 0.11 at 100 Hz. The small dielectric loss can be ascribed to the oxidized SiO_2 layers on the surface of Si cores, which prevent the direct contact between adjacent Si particles and thus block the transfer of free charge carriers. Therefore, it can be concluded that the SiO_2 coating layer plays a crucial role in suppressing dielectric loss of the Si*/epoxy composites. For the Si*@PDA/epoxy composite, PDA coating layer also plays as a similar role in blocking the transfer of free charge carriers. Moreover, the amino groups on the surface of PDA coating layer, capable of covalently reacting with the epoxy matrix, can efficiently crosslink the fillers and the matrix. A large amount of covalent bond formation hinders the transfer of free charge carriers, resulting in the reduction of dielectric loss. In this work, remarkable reduction of loss tangent is achieved by introducing SiO_2 and PDA insulating layers between Si cores, which avoid their direct contact. More importantly, the PDA layers can react with the epoxy matrix, forming a large number of covalent bonds, which further suppress the mobility of free charge carriers. It would be acceptable by slightly reducing dielectric permittivity to achieve low loss for practical application.

The dependence of the conductivity of the composites on the Si concentration near the percolation concentration (f_c) is described by a scaling law as follows:

$$\sigma \propto (f_c - f_{si})^{-s} \quad \text{for} \quad f_c \geq f_{si} \tag{2}$$

where σ is the conductivity of the epoxy composite, f_{Si} is the filling factor, f_c is the percolation threshold, and s is the critical exponent in the insulating region.

It is well known that the resistivity is the reciprocal of the conductivity. Fig. 6 shows the volume resistivity (R_V) for the three composite systems. Generally, variation of R_V at various conductive or semiconductive filler content is nonlinear [38]. This curve can be divided into three parts. In the initial region with low filler content, where particles are not in contact with each other, the R_V with filler content gradually decreases with the reductive distance between conductors or semiconductors. In the middle part near f_c, there is an abrupt decrease in resistivity. This means the particles are in good contact with each other. Beyond f_c, the change of R_V becomes steady. In this case, the tunneling resistance plays an important role in the electrical conductivity of composites filled with filler particles due to the unavoidable insulating film of matrix material between adjacent particles [39,40]. Therefore, the Rv of the composites is much higher than that of Si filler particles.

For the Si/epoxy composite, the R_V shows a distinct percolation phenomenon because of the significant reduction when the Si content reaches 33.8 vol%, and f_c is believed in a range between 25.5 and 33.8 vol%. However, the R_V values for Si*/epoxy and Si*@PDA/epoxy composites slightly decrease with the filler loading, and no obvious percolation phenomenon is found, indicating the insulating nature of the oxidized SiO_2 and coating PDA shell. The insulating shell can prevent the direct contact between the core Si particles and block the formation of current paths across the composites. Thus, electrons can only transmit through adjacent Si particles via inter-Si tunneling [1,37]. Therefore, the resistivity especially for the Si*@PDA/epoxy composite is considerably increased when compared with the Si/epoxy composite, while maintaining the same magnitude as the pure epoxy.

For a composite, dielectric loss, ε'' can be expressed as [13]:

$$\varepsilon'' = \varepsilon''_{dc} + \varepsilon''_{MW} + \varepsilon''_{D} \tag{3}$$

where ε''_{dc} and ε''_{MW} are related to conduction and interfacial polarization, respectively, and ε''_{D} stands for the dipole loss factor.

The conduction loss factor is given by

$$\varepsilon''_{dc} = \frac{\sigma_{dc}}{2\pi f} \tag{4}$$

As revealed in Fig. 5d, we can see that there is no noticeable contribution of conduction loss factor on the dielectric loss for the Si*/epoxy and Si*@PDA/epoxy composites, because no DC conductivity appears, thus leading to a low dissipation factor. Therefore, the f_c is surely greater than that of the Si*/epoxy and Si*@PDA/epoxy composites with 33.8 vol% filler content, owing to the insulating SiO_2 and PDA shell which effectively block the migration of the free carriers at the multiphase interface area. However, the DC conductivity is observed for the Si/epoxy composite, suggesting that the conduction loss is dominant in the low-frequency range. Therefore, the DC conductivity results in the large dissipation factor [5].

3.4. Thermal conductivity

In general, the thermal conductivity of the inorganic-organic composites greatly depends on the structure, loading amount, dispersity and surface characteristics of the inorganic fillers, as well as the interface thermal resistance between fillers and polymer matrices [13,37,41–48]. Fig. 7 compares the room temperature thermal conductivity of Si/epoxy, Si*/epoxy and Si*@PDA/epoxy composites with different filler volume fractions. The pure epoxy has a relatively low thermal conductivity of 0.183 W/m K at room temperature. When increasing the Si filler loading amounts from 5.4 vol% to 33.8 vol%, the thermal

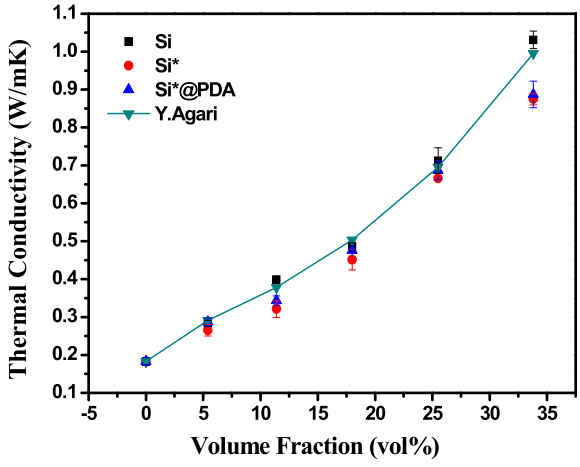

Fig. 7. Comparison of the experimental and theoretical values of the thermal conductivity of the three composites with different filler volume faction.

conductivity of the Si/epoxy composites are remarkably increased owing to the high thermal conductivity of Si (~148 W/m K). The result suggests that a weak interaction among thermally conductive Si particles presents at a lower filler content, which thus results in the low thermal conductivity due to the high interface thermal resistance. In contrast, Si particles can form partial connection or networks at a higher filler loading amount, which is beneficial for phonon transmission and thus capable of greatly increasing the thermal conductivity. The thermal conductivities of the composites with 33.8 vol% Si, Si* and Si*@PDA fillers are approximately 1.036 W/m K, 0.876 W/m K, and 0.891 W/m K, respectively, which are more than four times of that of the pure epoxy.

Referring to the previous studies [49,50], the epoxy composite with 3 wt% Exfoliated Graphite (EG) showed higher thermal conductivity (0.943 W/m K) than that of the composite with multiwall carbon nanotubes (MWCNTs). The planar structure of 2D EG significantly increased the interfacial contact area between the epoxy matrix and the EG filler. Moreover, EG had lager specific surface area than that of Si particles, which was easier to form a network even at low filler loading content. As compared with the Si*/epoxy and the Si*@PDA/epoxy composites, the Si/epoxy composite can be much more effective in enhancing its thermal conductivity at the same filler content, because the Si has higher intrinsic thermal conductivity than that of SiO_2 and PDA. In contrast, the thermal conductivity values of Si*@PDA/epoxy composites are larger than those of Si*/epoxy at the same filler content, but are slightly lower than that of those untreated Si/epoxy composites. The reason is that the surface of the functionalized PDA has plenty of amine groups, which can react with epoxy resin and enhance the interfacial adhesion between the filler and the epoxy matrix. The excellent interface compatibility effectively reduces the void production, which usually appears between the filler and epoxy matrix (Fig. 3), thus resulting in the reduction of the interface thermal resistance. Moreover, the thermal conductivity of the neat epoxy and the Si*@PDA/epoxy composites shows a rather weak temperature dependence, primarily owing to their high glass-transition temperature (Tg) and thermostability (Figs. S4–7). The incorporation of Si particles would enhance thermomechanical properties of epoxy matrix, which is consistent with the previous work [7]. Nanofillers have significant effect on the thermal and mechanical properties of polymer matrix [51–67]. Therefore, Si particles can be a promising filler material to reinforce the epoxy polymer matrix while largely preserving its thermal stability. Furthermore, surface treatment of Si particles can enhance the interfacial interactions between the Si fillers and the epoxy. The covalent bonding formation between Si particles and epoxy matrix can reduce the mobility of the local matrix material around the filler particles, thus increasing the thermal stability even at elevated temperatures [68,69].

The effective thermal conductivity of the Si/epoxy composites was further elucidated and analyzed by combining the experimental data and thermal conductivity model. On the basis of Y. Agari model [70], the theoretical equation below was used in this work to explore the influence of the fillers on thermal conductivity behavior of the composites.

$$\log K_c = \Phi_f \cdot C_2 \cdot \log K_f + 1 - \Phi_f \cdot \log C_1 \cdot K_m \quad (5)$$

where K_c, K_m and K_f represent the thermal conductivities of the composite, matrix and filler, respectively, and Φ_f is the volume fraction of the filler. C_1 is a factor regarding the effect of the filler on the secondary structure of the polymer, and C_2 relates to the degree of ease and difficulty in forming conductive chains of the filler. In eq. (5), logarithms of the thermal conductivity values of the composite linearly increase along with the volume fraction of the filler, while constants C_2 and C_1 are determined by the experimental measurement. As shown in Fig. 7, the predicted thermal conductivity values are well consistent with the experimental ones at low filler contents, and the deviation occurs at high filler content owing to the poor dispersion of the fillers and the voids produced within the composites, but which has not taken into account in the theoretical prediction. Among all the three composite systems, Agari model gives a good prediction for the thermal conductivity of the Si/epoxy composites and the calculated values are close to that of the experimental values.

4. Conclusions

In summary, we demonstrated the fabrication of three kinds of epoxy-based composites using Si, core-shell Si@SiO_2 (denoted as Si*) and core-shell-shell Si@SiO_2@PDA (denoted as Si*@PDA) as fillers, respectively, and systematically investigated their dielectric properties and thermal conductivities. It was found that the dielectric constant and the loss tangent increased with increasing filler loading amount in the three composites in a wide frequency range. As compared with Si/epoxy, the Si* and Si*@PDA fillers remarkably suppressed the dielectric loss tangent of the composites at the same filler fraction. The reason can be ascribed to the formation of the SiO_2 and the PDA shells on the surface of Si particle, which served as an insulating layer between the Si cores, thus preventing them from contacting with each other. Meanwhile, a remarkable reduction of dielectric loss tangent was achieved at a significantly reduced level of dielectric permittivity. The thermal conductivities of the epoxy-based composites increased with the increase of Si content in the three composites. The thermal conductivity of the Si*/epoxy was slightly lower than that of the Si/epoxy due to the lower thermal conductivity of the SiO_2 shell, which suppressed the phonon transfer. Interestingly, the thermal conductivity of Si*@PDA/epoxy slightly increased in comparison with that of the Si*/epoxy because the coated PDA layer effectively enhanced the interfacial adhesion between the Si*@PDA fillers and the epoxy matrix. Moreover, it's well recognized that the core-shell particle-based composites with high dielectric constant but low loss tangent, high thermal conductivity, Tg and storage modulus are very promising for embedded capacitors and structural capacitors.

Acknowledgments

The authors thank Mr Chuansheng Ma and Ms Yanzhu Dai at International Center for Dielectric Research (ICDR) of Xi'an Jiaotong University for the help with SEM/TEM measurements. We appreciate the support of Muhammad Junaid, who offers us significant help in grammar revision.

Appendix A. Supplementary data

Supplementary data related to this article can be found at http://dx.doi.org/10.1016/j.compositesb.2017.12.004.

References

[1] Zhou W, Yu D. Fabrication, thermal, and dielectric properties of self-passivated Al/epoxy nanocomposites. J Mater Sci 2013;48(22):7960–8.
[2] Dang ZM, Zheng MS, Zha JW. 1D/2D Carbon nanomaterial-polymer dielectric composites with high permittivity for power energy storage applications. Small 2016;12:1688–701.
[3] Lu J, Moon KS, Kim BK, et al. High dielectric constant polyaniline/epoxy composites via in situ polymerization for embedded capacitor applications. Polymer 2007;48(6):1510–6.
[4] Zhou WY, Chen QG, Sui XZ, Dong LN, Wang ZJ. Enhanced thermal conductivity and dielectric properties of Al/b-SiCw/PVDF composites. Compos Part A Appl Sci & Manuf 2015;71:184–91.
[5] Wan YJ, Zhu PL, Yu SH, et al. Barium titanate coated and thermally reduced graphene oxide towards high dielectric constant and low loss of polymeric composites. Compos Sci Technol 2017;141:48–55.
[6] Min C, Yu D, Cao J, et al. A graphite nanoplatelet/epoxy composite with high dielectric constant and high thermal conductivity. Carbon 2013;55(2):116–25.
[7] Sun W, Wu H, Tan X, et al. Silanized-silicon/epoxy nanocomposites for structural capacitors with enhanced electrical energy storage capability. Compos Sci Technol 2015;121:34–40.
[8] Goyal RK, Katkade SS, Mule DM. Dielectric, mechanical and thermal properties of polymer/BaTiO3, composites for embedded capacitor. Compos B Eng 2013;44(1):128–32.

[9] Prakash BS, Varma KBR. Dielectric behavior of CCTO/epoxy and Al-CCTO/epoxy composites. Compos Sci Technol 2007;67(11–12):2363–8.
[10] Hu T, Juuti J, Jantunen H, et al. Dielectric properties of BST/polymer composite. J Eur Ceram Soc 2007;27(13–15):3997–4001.
[11] Qi L, Lee B, Chen S, et al. High-dielectric-constant silver-epoxy composites as embedded dielectrics. Adv Mater 2005;17(14):1777–81.
[12] Shen Y, Lin Y, Li M, et al. High dielectric performance of polymer composite films induced by a percolating interparticle barrier layer. Adv Mater 2007;19(10):1418–22.
[13] Zhou W, Wang Z, Dong L, et al. Dielectric properties and thermal conductivity of PVDF reinforced with three types of Zn particles. Compos Part A Appl Sci & Manuf 2015;79:183–91.
[14] Zhang Y, Wang Y, Deng Y, et al. High dielectric constant and low loss in polymer composites filled by self-passivated zinc particles. Mater Lett 2012;72(4):9–11.
[15] Huang XY, Kim C, Jiang PK, Yin Y, Li Z. Influence of aluminum nanoparticle surface treatment on the electrical properties of polyethylene composites. J Appl Phys 2009;105:014105.
[16] Vivo BD, Guadagno L, Lamberti P, et al. Electromagnetic properties of carbon nanotube/epoxy nanocomposites[C]. International Symposium on Electromagnetic Compatibility-Emc Europe. IEEE; 2009. p. 1–4.
[17] Lu Y, Zhao Y, Yu L, et al. Hydrophilic Co@Au yolk/shell nanospheres: synthesis, assembly, and application to gene delivery. Adv Mater 2010;22(12):1407–11.
[18] Lee J, Ji CP, Song H. A nanoreactor framework of a Au@SiO_2 yolk/shell structure for catalytic reduction of p-nitrophenol. Adv Mater 2008;20(8):1523–8.
[19] Wu H, Wu G, Wang L. Peculiar porous α-Fe_2O_3, γ-Fe_2O_3 and Fe_3O_4 nanospheres: facile synthesis and electromagnetic properties. Powder Technol 2015;269:443–51.
[20] Wu H, Wu G, Ren Y, et al. Co/Co ratio dependence of electromagnetic wave absorption in hierarchical $NiCo_2O_4$-$CoNiO_2$ hybrids. J Mater Chem C 2015;3(29):7677–90.
[21] Wu G, Cheng Y, Ren Y, Wang Y, Wang Z, Wu H. Synthesis and characterization of γ-Fe_2O_3@C nanorod-carbon sphere composite and its application as microwave absorbing material. J Alloy Compd 2015;652:346–50.
[22] Wu G, Cheng YH, Xiang F, Jia ZR, Xie Q, Wu G, et al. Morphology-controlled synthesis, characterization and microwave absorption properties of nanostructured 3D CeO_2. Mater Sci in Semicon Proc 2016;41:6–11.
[23] Zhang L, Yuan S, Chen S, et al. Preparation and dielectric properties of core-shell structured Ag@polydopamine/poly(vinylidene fluoride) composites. Compos Sci Technol 2015;110:126–31.
[24] Huang X, Jiang P. Core–shell structured high-k polymer nanocomposites for energy storage and dielectric applications. Adv Mater 2015;27(3):546.
[25] Cui W, Du F, Zhao J, et al. Improving thermal conductivity while retaining high electrical resistivity of epoxy composites by incorporating silica-coated multi-walled carbon nanotubes. Carbon 2011;49(2):495–500.
[26] Xie L, Huang X, Huang Y, et al. Core-shell structured hyperbranched aromatic polyamide/$BaTiO_3$ hybrid filler for poly(vinylidene fluoride-trifluoroethylene-chlorofluoroethylene) nanocomposites with the dielectric constant comparable to that of percolative composites. ACS Appl Mater Inter 2013;5(5):1747.
[27] Ke Y, Huang X, Xie L, et al. Core-shell structured polystyrene/$BaTiO_3$ hybrid nanodielectrics prepared by in situ RAFT polymerization: a route to high dielectric constant and low loss materials with weak frequency dependence. Macromol Rapid Comm 2012;33(22):1921–6.
[28] Sun W, León JED, Ma C, et al. Novel Si/cyanate ester nanocomposites with multifunctional properties. Compos Sci Technol 2012;72(14):1692–6.
[29] Wu H, Kessler MR. Multifunctional cyanate ester nanocomposites reinforced by hexagonal boron nitride after noncovalent biomimetic functionalization. ACS Appl Mater Inter 2015;7(10):5915.
[30] Vivo BD, Lamberti P, Spinelli G, et al. A morphological and structural approach to evaluate the electromagnetic performances of composites based on random networks of carbon nanotubes. J Appl Phys 2014;115(15):3408–11.
[31] Gardea F, Lagoudas DC. Characterization of electrical and thermal properties of carbon nanotube/epoxy composites. Compos B Eng 2014;56(1):611–20.
[32] Tayfun U, Kanbur Y, Abaci U, et al. Mechanical, flow and electrical properties of thermoplastic polyurethane/fullerene composites: effect of surface modification of fullerene. Compos B Eng 2015;80:101–7.
[33] Liang GD, Tjong SC. Electrical properties of percolative polystyrene/carbon nanofiber composites. IEEE Dielect El In 2008;15(1):214–20.
[34] Costa P, Silva J, Ansón-Casaos A, et al. Effect of carbon nanotube type and functionalization on the electrical, thermal, mechanical and electromechanical properties of carbon nanotube/styrene–butadiene–styrene composites for large strain sensor applications. Compos B Eng 2014;61(52):136–46.
[35] Ishimoto K, Kanegae E, Ohki Y, et al. Superiority of dielectric properties of LDPE/MgO nanocomposites over microcomposites. IEEE Dielect El In 2009;16(6):1735–42.
[36] Tanaka T. Dielectric nanocomposites with insulating properties. IEEE Dielect El In 2005;12(5):914–28.
[37] Dang ZM, Zheng MS, Zha JW. 1D/2D carbon nanomaterial-polymer dielectric composites with high permittivity for power energy storage applications. Small 2016;12(13):1688–701.
[38] Zhou W, Gong Y, Tu L, et al. Dielectric properties and thermal conductivity of core-shell structured Ni@NiO/poly(vinylidene fluoride) composites. J Alloy Comp 2016;693:1–8.
[39] Li C, Thostenson ET, Chou TW. Dominant role of tunneling resistance in the electrical conductivity of carbon nanotube–based composites. Appl Phys Lett 2007;91(22):2837.
[40] Spinelli G, Giustiniani A, Lamberti P, et al. Numerical study of electrical behaviour in carbon nanotube composites. Inter J Appl Electrom Mech 2012;39(1):21–7.
[41] Wang Z, Cheng Y, Wang H, et al. Sandwiched epoxy–alumina composites with synergistically enhanced thermal conductivity and breakdown strength. J Mater Sci 2017;52(8):4299–308.
[42] Wu G, Cheng YH, Wang ZD, Wang KK, Feng AL. In situ polymerization of modified graphene/polyimide composite with improved mechanical and thermal properties. J Mater Sci-Mater El 2017;28(1):576–81.
[43] Pan C, Kou K, Jia Q, et al. Improved thermal conductivity and dielectric properties of hBN/PTFE composites via surface treatment by silane coupling agent. Compos B Eng 2017;111:83–90.
[44] Shi Z, Radwan M, Kirihara S, et al. Enhanced thermal conductivity of polymer composites filled with three-dimensional brushlike AlN nanowhiskers. Appl Phys Lett 2009;95(22):282.
[45] Jung H, Yu S, Bae NS, et al. High through-plane thermal conduction of graphene nanoflake filled polymer composites melt-processed in an L-shape kinked tube. ACS Appl Mater Inter 2015;7(28):15256.
[46] Nan CW, Liu G, Lin Y, et al. Interface effect on thermal conductivity of carbon nanotube composites. Appl Phys Lett 2004;85(16):3549–51.
[47] Guan FL, Gui CX, Zhang HB, et al. Enhanced thermal conductivity and satisfactory flame retardancy of epoxy/alumina composites by combination with graphene nanoplatelets and magnesium hydroxide. Compos B Eng 2016;98:134–40.
[48] Fukushima H, Drzal LT, Rook BP, et al. Thermal conductivity of exfoliated graphite nanocomposites. J Therm Anal Calorim 2006;85(1):235–8.
[49] Romano V, Naddeo C, Vertuccio L, et al. Experimental evaluation and modeling of thermal conductivity of tetrafunctional epoxy resin containing different carbon nanostructures. Polym Eng Sci 2017;57(7).
[50] Romano V, Naddeo C, Guadagno L, et al. Thermal conductivity of epoxy resins filled with MWCNT and hydrotalcite clay: experimental data and theoretical predictive modeling. Polym Compos 2015;36(6):1118–23.
[51] Khonakdar HA. Dynamic mechanical analysis and thermal properties ofLLDPE/EVA/modified silica nanocomposites. Compos B Eng 2015;76:343–53.
[52] Singh BP, Singh D, Mathur RB, et al. Influence of surface modified MWCNTs on the mechanical, electrical and thermal properties of polyimide nanocomposites. Nanoscale Res Lett 2008;3(11):444.
[53] Nogueira T, Botan R, Neto JCM, et al. Effect of layered double hydroxides on the mechanical, thermal, and fire properties of poly(methyl methacrylate) nanocomposites. Adv Polym Tech 2013;32(S1):E660–74.
[54] Achaby ME, Arrakhiz FE, Vaudreuil S, et al. Mechanical, thermal, and rheological properties of graphene-based polypropylene nanocomposites prepared by melt mixing. Polym Composite 2012;33(5):733–44.
[55] Gabr MH, Okumura W, Ueda H, et al. Mechanical and thermal properties of carbon fiber/polypropylene composite filled with nano-clay. Compos B Eng 2015;69:94–100.
[56] Li Y, Pan D, Chen S, et al. In situ polymerization and mechanical, thermal properties of polyurethane/graphene oxide/epoxy nanocomposites. Mater Design 2013;47(9):850–6.
[57] Alhuthali A, Low IM. Water absorption, mechanical, and thermal properties of halloysite nanotube reinforced vinyl-ester nanocomposites. J Mater Sci 2013;48(12):4260–73.
[58] Shin SE, Ko YJ, Bae DH. Mechanical and thermal properties of nanocarbon-reinforced aluminum matrix composites at elevated temperatures. Compos B Eng 2016;106:66–73.
[59] Alhuthali A, Low IM. Mechanical and fracture properties of halloysite nanotube reinforced vinyl-ester nanocomposites. J Appl Polym Sci 2013;130(3):1716–25.
[60] Zhao YH, Zhang YF, Wu ZK, et al. Synergic enhancement of thermal properties of polymer composites by graphene foam and carbon black. Compos B Eng 2016;84:52–8.
[61] Wu SY, Huang YL, Ma CCM, et al. Mechanical, thermal and electrical properties of multi-walled carbon nanotube/aluminium nitride/polyetherimide nanocomposites. Polym Int 2012;61(7):1084–93.
[62] Ning Z, Liu R, Elhajjar RF, et al. Micro-modeling of thermal properties in carbon fibers reinforced polymer composites with fiber breaks or delamination. Compos B Eng 2017;114:247–55.
[63] Zaman Haydar U, Park Deuk Hun, Khan Ruhul A, et al. Effect of monomer-treated inorganic fillers on mechanical, rheological, and thermal properties of LLDPE nanocomposites. Composite Interfaces 2012;19(1):15–27.
[64] Bidsorkhi HC, Soheilmoghaddam M, Pour RH, et al. Mechanical, thermal and flammability properties of ethylene-vinyl acetate (EVA)/sepiolite nanocomposites. Polymer Testing 2014;970(8):259–62.
[65] Zhao YH, Zhang YF, Bai SL, et al. Carbon fibre/graphene foam/polymer composites with enhanced mechanical and thermal properties. Compos B Eng 2016;94:102–8.
[66] Wei H, Chen Y, Zhang T, et al. Thermal, mechanical, and shape…emory properties of nanorubber-toughened, epoxy-based shape…emory nanocomposites. J Appl Polym Sci 2017;135:45780.
[67] Ning Z, Liu R, Elhajjar RF, et al. Micro-modeling of thermal properties in carbon fibers reinforced polymer composites with fiber breaks or delamination. Compos B Eng 2017;114:247–55.
[68] Yu J, Huang X, Wang L, et al. Preparation of hyperbranched aromatic polyamide grafted nanoparticles for thermal properties reinforcement of epoxy composites. Polym Chem-UK 2011;2(6):1380–8.
[69] Sahu M, Narashimhan L, Prakash O, et al. Non-covalently functionalized tungsten disulfide nanosheets for enhanced mechanical and thermal properties of epoxy nanocomposites. ACS Appl Mater Inter 2017;9(16).
[70] Agari Y, Uno T. Estimation on thermal conductivities of filled polymers. J Appl Polym Sci 2010;32(7):5705–12.